Role of viscosity coefficients during spreading and coalescence of droplets in liquids

Bibin M. Jose and Thomas Cubaud

Phys. Rev. Fluids **2**, 111601 — Published 10 November 2017

DOI: 10.1103/PhysRevFluids.2.111601

Role of Viscosity Coefficients during Spreading and Coalescence of Droplets in Liquids

Bibin M. Jose and Thomas Cubaud[1]

Department of Mechanical Engineering, Stony Brook University, Stony Brook, NY, 11794-2300, USA

(August 6, 2017)

Abstract

The role of absolute viscosities on the dynamics of droplet spreading on solids and droplet-droplet coalescence in liquid/liquid systems is experimentally characterized for broad range of fluid parameters. We show in particular the existence of a viscous function based on both inner and outer fluid viscosities that allows for the determination of the critical wetting velocity and the evolution of contact diameters during immersed spreading and coalescence of droplets. This work quantifies the cooperative effects of fluid viscosities on droplet dynamics as well as their overall reduced influence from initial wetting to spreading and coalescence, which provides insights into the role of wetting contact lines on spontaneous capillary phenomena.

PACS numbers: 47.55.D-, 47.55.df, 47.55.nk, 47.55.np

[1] Author to whom correspondence should be addressed.
Email address: thomas.cubaud@stonybrook.edu

Spontaneous capillary phenomena are widespread in nature and typically involve complex interfacial dynamics driven with surface tension. From the coalescence of water droplets in clouds to the dewetting of tires on wet roads [1], everyday life offers countless examples of interfacial fluid motion [2]. Although the spreading of liquids on solids has been widely investigated in air for coating applications and material characterization, liquid/liquid systems are often found in subsurface flows during oil recovery and constitutes the basis of emulsions. In this case, coalescence with walls or between droplets alters the quality of dispersions and is usually mitigated with the addition of surfactant. For simple fluids, interfacial and bulk properties are known to regulate droplet merging process and studies have shown the influence of capillary and Ohnesorge numbers on coalescence [3-9] and dynamic wetting [10-19]. As the balance between inertial, viscous, and surface tension forces is evolving during the process, various dimensionless quantities are used to describe different stages of droplet merging. When both fluids are viscous, the viscosity ratio between inner and outer phases is also used in the description of droplet coalescence [20] and droplet deformation and breakup in shear flows [21,22], however, an indetermination resides about the role of absolute viscosity coefficients on dynamics. In addition to its fundamental aspect, better understanding the cooperative effects of inner and outer viscosities on droplet behavior is needed for improving the manipulation of high-viscosity multiphase flows in microfluidic devices where coupling between natural and convective time-scales can lead to intriguing interfacial flow morphologies [23].

Here, we show the existence of a viscous function based on both inner and outer fluid viscosities that enables the determination of the critical wetting velocity and the evolution of both spreading and coalescing droplets for wide range of viscosity contrasts. In particular, we individuate the role of each viscosity by conducting an extensive series of experiments to clarify scaling laws of spontaneous capillary phenomena in liquid/liquid systems.

A goniometer equipped with a high-speed camera and a magnification scope is used to laterally visualize droplets during immersed spreading and coalescence experiments. Droplets are formed at the tip of calibrated capillary tubes that are connected to syringe pumps with flexible tubing and translated using microstages. The camera acquisition rate is adjusted between 50 and 4000 fps and the spatial resolution is measured using the capillary. Borosilicate glass substrates are treated in an oven at 400° C for an hour and cooled to room temperature before being placed inside a transparent cell filled with silicone oil. Water/glycerol droplets are then deposited by slowly lowering the capillary toward the solid surface and waiting until natural spreading occurs through rupture of the external film at the wall. The scope is slightly tilted (< 5°) to obtain the image of the droplet and its reflection on glass [Fig. 1(a)]. A fiber optic

light is adjusted on the back side to promote internal reflection inside the glass and enable clear image processing of droplet contours [Fig. 1(b)].

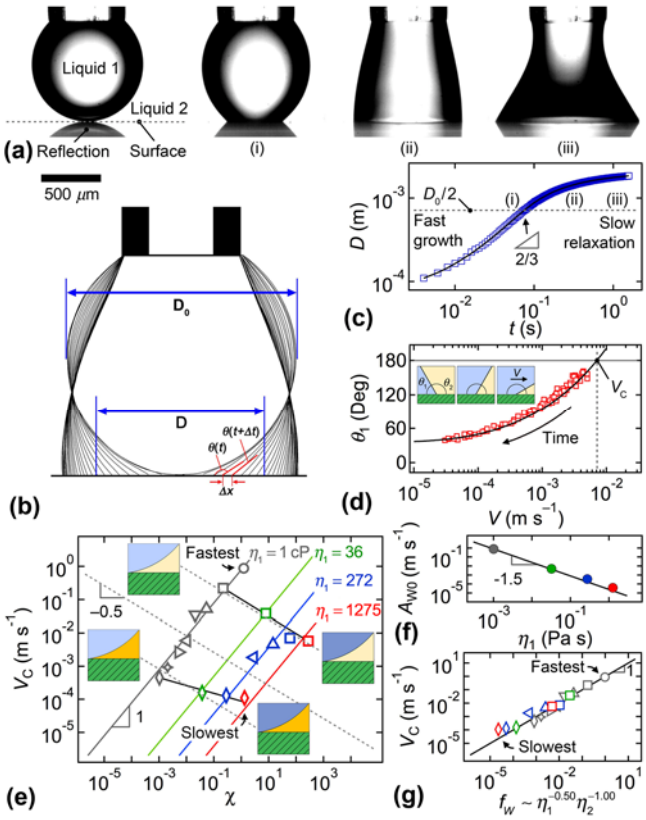

FIG. 1. (a) Micrographs of immersed droplet spreading on glass, fluid pair: G92-5 (b) Corresponding superimposed contours during spreading showing θ measurements. (c) Corresponding temporal evolution of contact diameter D. (d) Extrapolation of dynamic θ to calculate critical velocity V_C. (e) Phase diagram of V_C and viscosity contrast χ, solid lines for fixed η_1: $V_C = A_{W0}\chi$. (f) Prefactor A_{W0} vs. η_1, solid line: $A_{W0} = A_{W1}\eta_1^{-b}$, with $b = 1.5$ and $A_{W1} = 2.5\times10^{-5}$ m s^{-1}(Pa s)^b. (g) Comparison of V_C with Eq. (1).

Droplets are made of water-glycerol mixtures of dynamic viscosity η_1 and the external phase is composed of silicone oils of viscosity η_2 [Table I]. The fluid pairs display relatively uniform interfacial tension γ for broad variations of the viscosity contrast $\chi = \eta_1/\eta_2$ ranging between 10^{-3} and 10^3. We use a color code for the droplet viscosity and symbols designate the outer fluid. Viscosity is measured using tube viscometers and interfacial tension with a Du Nouy ring tensiometer. Given the relatively large capillary length associated with liquid-liquid systems $\lambda = [\gamma/(\Delta\rho g)]^{1/2}$, where $\Delta\rho$ is the difference in density between phases and g is the gravitational acceleration, droplets initially form spherical caps of diameter

D_0 that ranges between 0.45 and 3.5 mm. As the initial local interfacial curvature near fluid contact corresponds to $D_0/2$, the initial diameter D_0 is used to normalize the instantaneous width of the liquid bridge D during spreading and coalescence experiments. The temporal evolution of D is extracted from spatiotemporal analysis of the wetting front [Fig. 1(c)]. Similar to the case of spreading drops in air [12], the diameter of immersed droplets follows a scaling law according to $D \sim t^{\alpha}$, where the exponent α progressively decreases. The diameter rapidly grows for short times and a slow relaxation regime takes place for longer times. We find that the exponent $\alpha \approx 2/3$ provides good agreement with experimental data for all droplets around their mid-growth when $D = D_0/2$. Although the instant $t = 0$, when droplets make initial contact with the glass, is clearly identifiable from movies, the direct measurement of the initial velocity V_C is prone to inherent uncertainties due the narrow optical access, which prevents the detection of the edges of the liquid bridge at the early stage of formation. Therefore, we extrapolate V_C using dynamic contact angle measurements such as $V_C = V(\theta \approx 180°)$, where the velocity $V = \Delta x/\Delta t$ is calculated from contact line displacements Δx between two images that are Δt apart, and $\theta = (\theta_t + \theta_{t+\Delta t})/2$ is the mean contact angle [Fig. 1(b)]. To avoid misinterpretation of contact angles, we measure $\theta < 150°$ when the contact angle can be defined with least ambiguity. Dynamic contact angles are fitted with a form of the Cox-Voinov relationship, which provides a useful relationship to characterize the evolution of dynamic contact angles with velocity [24-26], according to $\theta^3 = \theta_0^3 + \omega V$ where θ_0 is the apparent equilibrium contact angle and w is a constant that depends on each fluid pair [Fig. 1(d)]. Since we find that for highly damped viscous systems, the full droplet relaxation can take up to 30 days, we estimate θ_0 from the lowest apparent advancing contact angle measured for each trial and w corresponds to the fitting parameter. This method permits the practical estimation of the maximal dewetting velocity of the external phase V_C independently of electing the inner or outer viscosity in the analysis of experimental data.

Fluid pair	γ (mN m^{-1})	η_1 (cP)	η_2 (cP)	ρ_1 (kg m^{-3})	Symbol
G0-1	40.7	1	0.82	998	○
G0-5	42.7	…	4.6	…	□
G0-20	…	…	19	…	△
G0-50	…	…	48	…	▽
G0-100	…	…	97	…	◁
G0-200	…	…	194	…	▷
G0-500	…	…	486	…	▯
G0-1k	…	…	971	…	◊
G80-5	29.7	36	4.6	1213	□

G80-1k	…	…	971	…	◊
G92-5	29.3	272	4.6	1239	□
G92-20	…	…	19	…	△
G92-100	…	…	97	…	◁
G92-1k	…	…	971	…	◊
G99-5	27.7	1275	4.6	1260	□
G99-1k	…	…	971	…	◊

Table I. Fluid pairs used for spreading experiments.

To reveal the influence of both fluid viscosities on the initial spreading velocity, we plot V_C over six decades of the viscosity contrast $\chi = \eta_1/\eta_2$ on Fig. 1(e) where a color–intensity code is used in schematics to illustrate either low- or high-viscosity fluids with a light or dark blue color for the droplet phase and a yellow color for the external phase. As data appear to align on an oblique grid pattern, we fit results with scaling laws of the form $V_C = A_{W0}\chi^a$, with $a = 1$ for fixed η_1 and varying η_2. The prefactor is subsequently fitted according to $A_{W0} = A_{W1}\eta_1^{-b}$, with $b = 1.5$ and $A_{W1} = 2.5\times10^{-5}$ m s^{-1}(Pa s)^b. This grid patterning method enables the formulation of a viscous wetting function

$$f_W = A_{W1}\eta_1^{-1/2}\,\eta_2^{-1}, \qquad (1)$$

which permits a direct quantitative comparison of the influence of viscosities on the initial wetting velocity. In Fig. 1(g), we show the overall good agreement between velocity data and f_W for about four decades. Data demonstrate in particular the prominence of the viscosity of the external phase η_2 over the droplet viscosity η_1. The wetting function f_W also provides a reference for studying the viscosity contrast map with the calculation of expected V_C for fixed η_2 and varying η_1 according to $V_C(\eta_2) = A_1\chi^{-b+a}\eta_2^{-b}$, which is represented with dashed-lines on Fig. 1(e) and shows agreement with data.

Assuming a contact diameter according to $D \sim A_S t^\alpha$, the prefactor A_S plays a critical role in determining the order of magnitude of the droplet growth rate while the nearly constant $\alpha = 2/3$ for mid-growth fine tunes the diameter evolution. Hence, our method consists in probing the relationship of A_S with fluid viscosities. While the initial droplet diameter D_0 provides a natural normalization length-scale, interfacial tension γ drives both spreading and coalescence phenomena and time can be scaled with a viscous capillary time $\tau_V = \eta D_0/\gamma$ or an inertial capillary time $\tau = (\rho_1 D_0^3/\gamma)^{1/2}$. The inertial capillary time τ is independent of η and used as the reference time to probe the influence of viscosities for each fluid pair in our study.

The normalized temporal evolution of contact diameters of water droplets in silicone oils is shown in Fig. 2(a). Although the measured exponent α fluctuates across the viscosity contrast χ at mid-growth [Fig. 2(b)], the use of $\alpha = 2/3$ for $D = D_0/2$ provides a consistent technique to estimate A_S for all fluid pairs. Multiple experiments are conducted for each fluid pair, which results in a range of initial diameters D_0 for uniform growth coefficients A_S [Fig. 2(c)]. Indeed, the expression $D/D_0 = A_S(t/\tau)^{2/3}$ suggests that $D = A_S(\gamma/\rho)^{1/3}t^{2/3}$ with A_S being a function of η_1 and η_2. The mapping of A_S with the viscosity contrast $\chi = \eta_1/\eta_2$ is displayed in Fig. 2(d). A grid patterning method similar to our previous analysis of the critical velocity V_C is employed to individuate the role of each viscosity. We find in particular that for fixed η_1 and varying η_2, data are well fit with $A_S = A_{S0}\chi^a$ with $a = 0.67$ and the coefficient $A_{S0} = A_{S1}\eta_1^{-b}$, with $b = 0.87$ and $A_{S1} = 5.4\times10^{-3}$ (Pa s)^b [Fig. 2(e)]. This allows us to define a viscous spreading function proportional to $\eta_1^{-b+a}\eta_2^{-a}$ according to

$$f_S = A_{S1}\eta_1^{-1/5}\eta_2^{-2/3}, \qquad (2)$$

which shows good agreement with $A_S = f_S$ for two orders of magnitude [Fig. 2(f)]. We also calculate $A_S(\eta_2) = A_{S1}\eta_2^{-b}\chi^{-b+a}$ and plot with dashed-lines the expected curves of three corresponding external phase viscosities in relative good agreement with data [Fig. 2(d)].

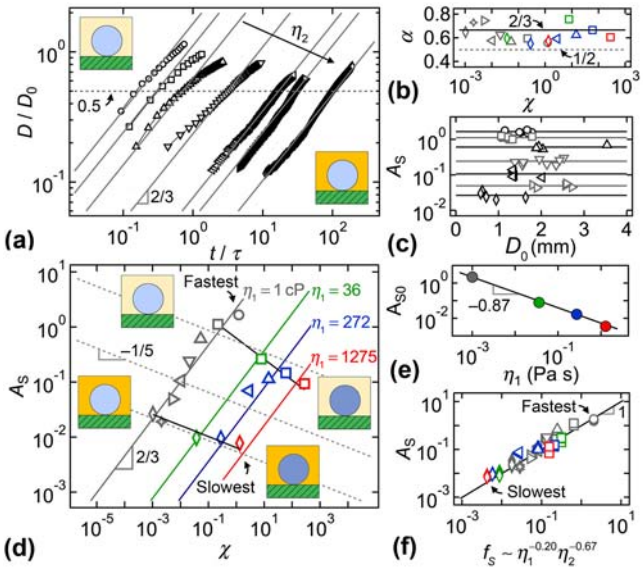

FIG. 2 (a) Normalized temporal evolution of spreading diameters of water droplets in silicone oils, solid lines: $D/D_0 = A_S(t/\tau)^{2/3}$. (b) Measured exponents α as a function of viscosity ratio χ around $D_0/2$, solid line $\alpha = 2/3$, dashed-line $\alpha = 1/2$. (c) Uniform growth coefficient A_S for various initial droplet size D_0. (d) Grid patterning of A_S with χ. Solid lines for fixed η_1: $A_S = A_{S0}\chi^{0.67}$ (e) Evolution of A_{S0} with droplet viscosity

η_1, solid line $A_{S0} = A_{S1}\eta_1^{-b}$ with $b = 0.87$ and $A_{S1} = 5.4\times10^{-3}$ (Pa s)^b (f) Comparison of growth factor A_S with Eq. (2).

Immersed droplet-droplet coalescence experiments are similarly implemented. Capillary tubes are aligned along their axis in a cell filled with liquid and a pendant droplet of size D_1 is slowly displaced toward a droplet of comparable size D_2 [Fig. 3(a)]. The average droplet size $D_0 = (D_1+D_2)/2$ is used to scale D and measurements of growth rates are conducted when $D \sim D_0/2$ using the fluid pairs shown in Table II. Data are treated to extract interfacial contours during coalescence [Fig. 3(b)]. The evolution of the liquid bridge follows a scaling of the form $D/D_0 = A_C(t/\tau)^\alpha$, where the growth coefficient A_C depends on viscosities [Fig. 3(c)] and the exponent α is close to 2/3 [Fig. 3(d)]. The phase diagram of A_C as a function of χ displays a typical grid pattern that reveals the cooperative influence of absolute viscosities. In particular, data for fixed η_1 and varying η_2 are fitted with $A_C = A_{C0}\chi^a$ where $a = 0.50$ and $A_{C0} = A_{C1}\eta_1^{-b}$ with $b = 0.60$ and $A_{C1} = 1.4\times10^{-1}$ (Pa s)^b [Fig. 3(e)]. The viscous coalescence function defined as,

$$f_C = A_{C1}\eta_1^{-1/10}\eta_2^{-1/2}, \qquad (3)$$

is found to collapse growth rates onto a master curve such as $A_C = f_C$. A crisscrossing calculation of the expected behavior of A_C for a fixed external phase viscosity η_2 yields $A_C(\eta_2) = A_{C1}\eta_2^{-0.6}\chi^{-0.1}$, which closely matches data for large η_1 and η_2. By contrast, for relatively low viscosities, the inviscid coalescence regime [7,27] independent of viscosities is recovered [Fig. 3(e)].

Fluid pair	γ (mN m^{-1})	η_1 (cP)	η_2 (cP)	ρ_1 (kg m^{-3})	Symbol
G0-100	42.7	1	97	998	◀
G0-1k	…	…	971	…	♦
G0-10k	…	…	9710	…	◆
G80-100	29.7	36	97	1213	◀
G80-1k	…	…	971	…	♦
G80-10k	…	…	9710	…	◆
G80-30k	…	…	29,280	…	◢
G92-100	29.3	272	97	1239	◀
G92-1k	…	…	971	…	♦
G92-10k	…	…	9,710	…	◆
G92-30k	…	…	29,280	…	◢
G99-100	27.7	1275	97	1260	◀
G99-1k	…	…	971	…	♦

G99-10k	…	…	9710	…	◆
G99-30k	…	…	29280	…	◢

Table II. Fluid pairs used in coalescence experiments.

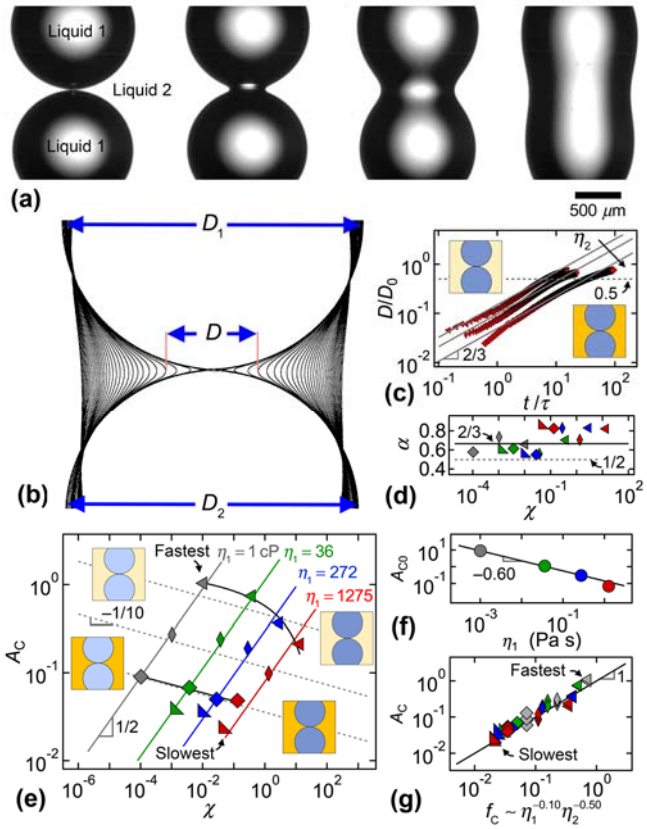

FIG. 3. (a) Micrographs of coalescing droplets, fluid pair: G0-10k (b) Superimposed contours of coalescing droplets, fluid pair: G80-10k. (c) Normalized temporal evolution of D for glycerol drops, solid line $D/D_0 = A_C(t/\tau)^{2/3}$. (d) Measured initial α as a function of χ, solid line $\alpha = 2/3$, dashed-line $\alpha = 1/2$. (e) Phase diagram of A_C with χ, solid lines for fixed η_1: $A_C = A_{C0}\chi^{0.5}$. (f) Evolution of A_{S0} with droplet viscosity η_1, solid line $A_{C0} = A_{C1}\eta_1^{-b}$ with $b = 0.60$ and $A_{C1} = 1.4\times10^{-1}$ (Pa s)^b. (g) Comparison of A_C with Eq. (3).

The similarity in the mathematical formulation of D for both spreading and coalescence enables a direct comparison between A_S and A_C to gain quantitative insights into the influence of wetting contact lines. For a given fluid pair, the dimensionless time τ_S required for a spreading droplet to reach its mid-growth corresponds to $(2A_S)^{-3/2}$ while the time $\tau_C = (2A_C)^{-3/2}$ is required for mid-coalescence. Therefore,

the time scale ratio $\tau_S/\tau_C = (A_C/A_S)^{3/2} = [\eta_1^{0.1}\eta_2^{0.17}A_{C1}/A_{S1}]^{3/2}$ is an increasing function of viscosities due to the more marked influence of viscosities in the presence of a solid surface for spreading. This behavior is recovered in the data where $\tau_S/\tau_C = 33$ for fluid pair G0-10k and $\tau_S/\tau_C = 144$ for fluid pair G99-10k, indicating that, in all cases, coalescence is much faster than spreading for similar fluid pairs.

Our work shows the combined yet asymmetrical influence of liquid viscosities during immersed spreading and coalescence of droplets in liquids. We address the two-viscosity problem of liquid/liquid systems by introducing a viscous function based on the product of inner and outer viscosity coefficients raised to various exponents for each phenomenon and show good agreement with data over multiple orders of magnitude. While the viscosity ratio provides a measure of relative viscosity, the proposed viscous function characterizes the role of absolute viscosities on droplet merging processes. The actual cooperation between fluid viscosities is evident based on the fact that viscosity exponents have the same sign in the formulation of *f*. In particular, the exponent associated with the viscosity of the external phase is at least twice larger than that of the droplets and the overall viscous contribution depends on the magnitude of the exponent *b*, which decreases from initial wetting, to spreading and coalescence. Given the experimental nature of our inquiry, we recognize the inherent need for complementary modelling work to fully characterize the values of proposed exponents, the uncertainty of which is estimated to be on the order of ten percent. Although the phenomena of droplet spreading and coalescence are well-known in air, experimental, theoretical, and numerical characterization of the viscous function *f* would allow to better elucidate the role of each fluid property on interfacial dynamics of liquid/liquid systems.

We have appreciated discussions with Laurent Limat and Carlos Colosqui. This material is based upon work supported by the National Science Foundation under Grants No. CBET-1150389 and No. CBET-1605809.

[1] F. Brochard-Wyart and P. G. de Gennes, Dewetting of a water film between a solid and a rubber, J. Phys.: Condens. Matter **6**, A9 (1994).
[2] J. Eggers, Nonlinear dynamics and breakup of free-surface flows, Rev. Mod. Phys. **69**, 865 (1997).
[3] J. Eggers, J. R. Lister, and H. A. Stone, Coalescence of liquid drops, J. Fluid Mech. **401**, 293 (1999).
[4] H. Aryafar and H. P. Kavehpour, Drop coalescence through planar surfaces, Phys Fluids **18**, 072105 (2006).
[5] K. Fezzaa and Y. Wang, Ultrafast X-ray phase-contrast imaging of the initial coalescence of two water droplets, Phys. Rev. Lett. **100**, 104501 (2008).
[6] Y. Yoon, M. Borrell, C. C. Park, and L. G. Leal, Viscosity ratio effects on the coalescence of two equal-sized drops in a two-dimensional linear flow, J. Fluid Mech. **525**, 355 (2005).

[7] J. D. Paulsen, R. Carmigniani, K. A., J. C. Burton, and S. R. Nagel, Coalescence of bubbles and drops in an outer fluid, Nature **5**, 3182 (2014).
[8] J. D. Paulsen, Approach and coalescenceof liquid drops in air, Phys. Rev. E **88**, 063010 (2013).
[9] J. D. Paulsen, J. C. Burton, and S. R. Nagel, Viscous inertial crossover in liquid drop coalescence, Phys. Rev. Lett. **106**, 114501 (2011).
[10] J. Eggers, Existence of receding and advancing contact lines, Phys Fluids **17**, 082106 (2005).
[11] L. H. Tanner, The spreading of silicone oil drops on horizontal surfaces, J. Phys. D: App. Phys. **12**, 1473 (1979).
[12] A. Eddi, K. G. Winkels, and J. H. Snoeijer, Short time dynamics of viscous drop spreading, Phys Fluids **25**, 013102 (2013).
[13] A. L. Biance, C. Clanet, and D. Quere, First steps in the spreading of a liquid droplet, Phys. Rev. E **69**, 016301 (2004).
[14] L. Courbin, J. C. Bird, M. Reyssat, and H. A. Stone, Dynamics of wetting: from inertial spreading to viscous imbibition, J. Phys. Condens. Matter **21**, 464127 (2009).
[15] J. C. Bird, S. Mandre, and H. A. Stone, Short-time dynamics of partial wetting, Phys. Rev. Lett. **100**, 234501 (2008).
[16] D. Seveno, T. D. Blake, S. Goossens, and J. De Coninck, Predicting the wetting dynamics of a two-liquid system, Langmuir **27**, 14958 (2011).
[17] A. Carlson, G. Bellani, and G. Amberg, Universality in dynamic wetting dominated by contact-line friction, Phys. Rev. E **85**, 045302 (2012).
[18] B. M. Jose and T. Cubaud, Formation and dynamics of partially wetting droplets in square microchannels, RSC Advances **4**, 14962 (2014).
[19] J. H. Snoeijer and B. Andreotti, Moving contact lines: scales, regimes, and dynamical transitions, Annu. Rev. Fluid Mech. **45**, 269 (2013).
[20] L. G. Leal, Flow induced coalescence of drops in a viscous fluid, Phys Fluids **16**, 1833 (2004).
[21] J. M. Rallison, The deformation of small viscous drops and bubbles in shear flows, Ann. Rev. Fluid Mech. **16**, 45 (1984).
[22] H. A. Stone, Dynamics of drop deformation and breakup in viscous fluids, Annu. Rev. Fluid Mech. **26**, 65 (1994).
[23] T. Cubaud, Wetting and lubricating film instabilities in microchannels, Phys Fluids **21**, 091103 (2009).
[24] O. V. Voinov, Hydrodynamics of wetting, Fluid Dyn. **11**, 714 (1976).
[25] R. G. Cox, Inertial and viscous effects on dynamic contact angles, J. Fluid Mech. **357**, 249 (1998).
[26] M. Fermigier and P. Jenffer, An experimental investigation of dynamic contact angle in liquid-liquid systems, J. Colloid Interface Sci. **146**, 227 (1991).
[27] M. Wu, T. Cubaud, and C.-M. Ho, Scaling law in liquid drop coalescence driven by surface tension, Phys Fluids **16**, L51 (2004).